Ab initio study of anharmonicity in high pressure Cmca-4 metallic hydrogen

Patricia Riego Saavedra

Supervised by A. Bergara and A. Leonardo

24th June 2014

Contents

Introduction

Hydrogen is the only atom for which the Schrödinger equation is solvable. Consisting only of a proton and an electron, hydrogen is the lightest element and, nevertheless, is far from being simple. Under ambient conditions, it forms diatomic molecules H_2 in gas phase, but different temperature and pressures lead to a complex phase diagram, which is not completely known yet. Solid hydrogen was first documented in 1899 [1] and was found to be isolating. At higher pressures, however, hydrogen can be metallized. In 1935 Wigner and Huntington predicted that the metallization pressure would be 25 GPa [2], where molecules would disociate to form a monoatomic metal, as alkali metals that lie below hydrogen in the periodic table. The prediction of the metallization pressure turned out to be wrong: metallic hydrogen has not been found yet, even under a pressure as high as 320 GPa. Nevertheless, extrapolations based on optical measurements suggest that a metallic phase may be attained at 450 GPa [3].

The interest of material scientist in metallic hydrogen can be attributed, at least to a great extent, to Ashcroft, who in 1968 suggested that such a system could be a high-temperature superconductor [4]. The temperature at which this material would exhibit a transition from a superconducting to a non-superconducting state (T_c) was estimated to be around room temperature. The implications of such a statement are very interesting in the field of astrophysics: in planets that contain a big quantity of hydrogen and whose temperature is below T_c, superconducting hydrogen may be found, specially at the center, where the gravitational pressure is high. This might be the case of Jupiter, whose proportion of hydrogen is about 90%. There are also speculations suggesting that the high magnetic field of Jupiter is due to persistent currents related to the superconducting phase [5]. Metallization and superconductivity of hydrogen has puzzled scientists for decades, and the community is trying to answer several questions. For instance, what is the structure of hydrogen at very high pressures? Or a more general one: what is the maximum T_c a phonon-mediated superconductor can have [6]?

A great experimental effort has been carried out pursuing metallic hydrogen and trying to answer the questions above; however, the characterization of solid phases of hydrogen is a hard task. Achieving the high pressures needed to get the sought phases requires advanced technologies. Diamond anvil cells (DAC) are commonly used devices. These devices consist of two diamonds with a tip of small area; for this reason, when a force is

applied, the pressure exerted is very big. This pressure is uniaxial, but it can be turned into hydrostatic pressure using transmitting media. Nowadays, this method makes it possible to reach pressures higher than 300 GPa, but even at this pressure hydrogen does not show metallic properties. A recently developed technique that is an improvement of DAC can reach pressures as high as 600 GPa [7], so it is a promising step forward in high pressure physics. Another drawback is that the electronic density of the structures is so low that X-ray diffraction patterns have low resolution. For these reasons, *ab initio* studies are an important source of knowledge in this field, within their limitations. When treating hydrogen, there are many subtleties in the calculations: as the atoms are so light, the ions forming the crystalline lattice have significant displacements even when temperatures are very low, and even at T=0 K, due to Heisenberg's uncertainty principle. Thus, the energy corresponding to this zero-point (ZP) motion is significant and has to be included in an accurate determination of the most stable phase. This has been done including ZP vibrational energies within the harmonic approximation for a range of pressures and at T=0 K, giving rise to a series of structures that are stable in their respective pressure ranges [8]. Very recently, a treatment of the phases of hydrogen that includes anharmonicity in ZP energies has suggested that relative stability of the phases may change with respect to the calculations within the harmonic approximation [9].

Many of the proposed structures for solid hydrogen have been investigated. Particularly, the *Cmca*-4 structure, which was found to be the stable one from 385-490 GPa [8], is metallic. Calculations for this structure, within the harmonic approximation for the ionic motion, predict a T_c up to 242 K at 450 GPa [10]. Nonetheless, due to the big ionic displacements, the harmonic approximation may not suffice to describe correctly the system. The aim of this work is to apply a recently developed method to treat anharmonicity, the stochastic self-consistent harmonic approximation (SSCHA) [11], to *Cmca*-4 metallic hydrogen. This way, we will be able to study the effects of anharmonicity in the phonon spectrum and to try to understand the changes it may provoque in the value of T_c.

The work is structured as follows. First we present the theoretical basis of the calculations: Density Functional Theory (DFT) for the electronic calculations, phonons in the harmonic approximation and the SSCHA. Then we apply these methods to *Cmca*-4 hydrogen and we discuss the results obtained. In the last chapter we draw some conclusions and propose possible future work.

Chapter 1

Theory

The description of a crystalline solid is a hard task due to the many-body nature of the problem. The formalism that applies in this case is Quantum Mechanics: in principle, one should solve the Schrödinger equation for the N electrons and the M ions present in the solid:

$$H\Psi_j(\mathbf{r}_1, ..., \mathbf{r}_N, \mathbf{R}_1, ..., \mathbf{R}_M) = E_j\Psi_j(\mathbf{r}_1, ..., \mathbf{r}_N, \mathbf{R}_1, ..., \mathbf{R}_M). \tag{1.1}$$

The wave function $\Psi_j(r_1, ..., \mathbf{r}_N, \mathbf{R}_1, ..., \mathbf{R}_M)$ is an eigenfunction of the Hamiltonian of the system with eigenvalue E_j and has all the information about the electrons and the ions. In the nonrelativistic case, which is the one we shall restrict to, the Hamiltonian governing the interactions in the solid is the following one (in Gaussian units):

$$\begin{aligned} H = &-\sum_i^N \frac{\hbar^2}{2m_e}\nabla_i^2 - \sum_j^M \frac{\hbar^2}{2m_j}\nabla_j^2 - \sum_i^N\sum_j^M \frac{Z_j e^2}{|\mathbf{r}_i - \mathbf{R}_j|} \\ &+ \sum_{i\neq j}^N \frac{1}{2}\frac{e^2}{|\mathbf{r}_i - \mathbf{r}_j|} + \sum_{i\neq j}^M \frac{1}{2}\frac{Z_i Z_j e^2}{|\mathbf{R}_i - \mathbf{R}_j|} \\ &= T_e + T_I + V_{e,I} + V_{e,e} + V_{I,I}. \end{aligned} \tag{1.2}$$

Here m_e is the mass of the electron, m_j the mass of the j^{th} ion, and Z_i and Z_j the atomic number of the i^{th} and j^{th} ions respectively. T_e and T_I are the electronic and ionic kinetic energy, respectively, and $V_{e,I}$, $V_{e,e}$ and $V_{I,I}$ are the electron-ion, electron-electron and ion-ion potential energy. Solving the eigenvalue problem for this Hamiltonian would provide us with an accurate description of the solid; nevertheless, we are handling a differential equation of $3(N+M)$ coupled degrees of freedom which is not exactly solvable. Even a numerical approach is out of reach, as the number of particles involved is of the order of Avogadro's number N_A ($N, M \sim 10^{23}$).

1.1 Born-Oppenheimer approximation

The first approximation that is usually made to simplify the problem is the so-called Born-Oppenheimer approximation, which is based on the fact that the electrons are much lighter than the ions[1]. So as to say, the movement of the electrons is much faster than that of the ions and thus their wave function can accomodate to the positions of the ions instantaneously. This allows us to uncouple the electronic and ionic degrees of freedom:

$$\Psi(r_1, ..., \mathbf{r}_N, \mathbf{R}_1, ..., \mathbf{R}_M) = \psi(r_1, ..., \mathbf{r}_N; \mathbf{R}_1, ..., \mathbf{R}_M)\phi(\mathbf{R}_1, ..., \mathbf{R}_M). \tag{1.3}$$

ψ is the electronic wave function and ϕ is the ionic one. The semicolon that separates the electronic and ionic coordinates in the electronic wave function denotes that, following the arguments made, ionic positions can be treated as parameters and not as variables when the motion of the electrons is being studied. The equation satisfied by ψ for a given set of ionic positions $\{\mathbf{R}_1, ..., \mathbf{R}_M\}$ is:

$$H_e\psi(r_1, ..., \mathbf{r}_N; \mathbf{R}_1, ..., \mathbf{R}_M) = E_e(\mathbf{R}_1, ..., \mathbf{R}_M)\psi(r_1, ..., \mathbf{r}_N; \mathbf{R}_1, ..., \mathbf{R}_M), \tag{1.4}$$

with

$$H_e = T_e + V_{e,e} + V_{e,I} \tag{1.5}$$

.

For the ionic motion, the equation satisfied by ϕ is:

$$H_I\phi(\mathbf{R}_1, ..., \mathbf{R}_M) = E_I\phi(\mathbf{R}_1, ..., \mathbf{R}_M), \tag{1.6}$$

with

$$H_I = T_I + V_{I,I} + E_e(\mathbf{R}_1, ..., \mathbf{R}_M). \tag{1.7}$$

It should be noted that the electronic energy enters the equation satisfied by the ionic wave function. Thus, if our aim is to study the ionic motion, the first step consists in the analysis of the electronic problem. Nonetheless, the electronic problem is still intractable, as it consists of $3N$ degrees of freedom coupled by the the electron-electron Coulomb interaction $V_{e,e}$: the problem has to be subject to further simplifications.

1.2 Density Functional Theory (DFT)

We now focus on the electronic problem, described by ψ. One of the most popular methods in *ab initio* electronic structure calculations, and the one used throughout this

[1] $m_{ions} \sim 10^3 m_e$.

work, is the so-called Density Functional Theory (DFT), introduced by Hohenberg and Kohn in 1964 [12]. In this formalism, the electronic density emerges as the key variable:

$$\begin{aligned} n(\mathbf{r}) =& \langle\psi| \sum_{i}^{N} \delta(\mathbf{r}-\mathbf{r}_i) |\psi\rangle \\ =& N \int \mathrm{d}\mathbf{r}_2 ... d\mathbf{r}_N \psi^*(\mathbf{r},\mathbf{r}_2,...,\mathbf{r}_N)\psi(\mathbf{r},\mathbf{r}_2,...,\mathbf{r}_N). \end{aligned} \tag{1.8}$$

If we integrate the density, we get the number of electrons: $N = \int \mathrm{d}\mathbf{r} n(\mathbf{r})$.

We will see in the next section that the ground state electronic density of a system determines all its electronic properties, so in principle any physical observable may be written in terms of n. The advantage is clear: we have passed from a complex function of 3N variables (the wave function ψ) to the density, a real function of just 3 variables.

1.2.1 Hohenberg-Kohn theorems

In their 1964 paper Hohenberg and Kohn proved the following theorems [12]:

- 1^{st} **theorem**: For any system of interacting particles in an external potential $V_{ext}(\mathbf{r})$, the potential $V_{ext}(\mathbf{r})$ is determined uniquely (except for an additive constant) by the ground state density of the system $n_0(\mathbf{r})$[2].

  - 1^{st} **corolary**: Due to the one-to-one relationship between the external potential and the ground state density, the Hamiltonian is completely determined (up to an additive constant) by the ground state density. And as the Hamiltonian of a system completely determines its properties, any electronic property p is a functional of $n_0(\mathbf{r})$. The drawback is that the expressions for $p[n_0(\mathbf{r})]$ are unknown, except for a few properties.

- 2^{nd} **theorem**: The total energy of the system can be written as a functional of the density ($E[n]$) for any external potential $V_{ext}(\mathbf{r})$. The exact ground state energy is the global minimum of this functional, and the density that minimizes it is the exact ground state density $n_0(\mathbf{r})$. The functional can be written as

$$E[n] = F[n] + \int \mathrm{d}\mathbf{r} V_{ext} n(\mathbf{r}), \tag{1.9}$$

  where $F[n]$ is a universal functional depending only on the kinetic energy and the internal potential energy of the interacting particles.

[2]The proof proceeds in two steps and by *reductio ad absurdum* [12], [14]: first it is shown that two different potentials cannot produce the same ground state wave function, as they satisfy different Schrödinger equations; second, it is shown that two different wave functions lead to different ground state densities.

- 2^{nd} **corolary**: The $E[n]$ functional alone suffices to determine the ground state energy and density.

We stress that in the specific problem of the electronic structure of a solid, the external potential is $V_{e,I}$ and the electron-electron interaction is the Coulomb energy $V_{e,e}$.

1.2.2 Kohn-Sham formulation

Once the Hohenberg-Kohn theorems have been presented, a practical scheme for their applicability is provided by the Kohn-Sham formulation [13].

For a better understanding of what follows, let us consider for a moment a system of noninteracting electrons. For such system (1.9) reads:

$$E_{ni}[n] = T_{ni}[n] + \int \mathrm{d}\mathbf{r} V_{ni}(\mathbf{r}) n(\mathbf{r}), \tag{1.10}$$

where $T_{ni}[n]$ denotes the noninteracting kinetic energy and V_{ni} is the external potential. That is, the $F[n]$ universal functional in (1.9) is just $T_{ni}[n]$ in the particular case of a system of noninteracting particles. There is no closed expression for $T_{ni}[n]$, but as we shall see, we do not need it, as it can be treated exactly if single-particle orbitals are introduced.

To minimize the energy with respect to the density, we take the functional derivative with respect to n in (1.10) and we introduce a Lagrange multiplier μ to ensure that the number of particles N remains constant. Proceeding this way, we get the equation:

$$\frac{\delta}{\delta n(\mathbf{r})}\left(E_{ni}[n] - \mu \int \mathrm{d}\mathbf{r} n(\mathbf{r})\right) = \frac{\delta T_{ni}[n]}{\delta n(\mathbf{r})} + V_{ni}(\mathbf{r}) - \mu = 0. \tag{1.11}$$

But on the other hand, we do know how to solve a system of noninteracting electrons. First, we have to solve the Schrödinger equation for a single particle and get the single-particle orbitals ϕ_j:

$$\left(-\frac{\hbar^2}{2m_e}\nabla_j^2 + V_{ni}(\mathbf{r})\right)\phi_j(\mathbf{r}) = \epsilon_j \phi_j(\mathbf{r}). \tag{1.12}$$

Second, the total wave function has to be constructed with a Slater determinant out of the single-particle orbitals, because electrons are fermions, so the total wave function has to be antisymmetric under the exchange of any two fermions.

$$\psi(\mathbf{r}_1, ..., \mathbf{r}_N) = \frac{1}{\sqrt{N!}} \begin{vmatrix} \phi_1(\mathbf{r}_1) & \phi_1(\mathbf{r}_2) & ... & \phi_1(\mathbf{r}_N) \\ \phi_2(\mathbf{r}_1) & \phi_2(\mathbf{r}_2) & ... & \phi_2(\mathbf{r}_N) \\ . & . & ... & . \\ . & . & ... & . \\ \phi_N(\mathbf{r}_1) & \phi_N(\mathbf{r}_2) & ... & \phi_N(\mathbf{r}_N) \\ . & & & \end{vmatrix} \tag{1.13}$$

It can be shown that the density (1.8) can be written as

$$n_0(\mathbf{r}) = 2\sum_{j}^{N_o} |\phi_j(\mathbf{r})|^2, \tag{1.14}$$

where N_o denotes the number of complete orbitals, each of them doubly occupied due to the spin degeneracy. So we can get the density out of the orbitals that are solutions of (1.12) with no need to treat explicitly $T_{ni}[n]$.

In order to implement DFT as an efficient method, Kohn and Sham [13] proposed to take advantage of the single-particle picture. The idea is simple: we compare a system of interacting electrons (the one we want to solve), which has a given ground state density $n_0(\mathbf{r})$, with an auxiliary system of noninteracting electrons that gives rise to the same density.

For an interacting system of electrons (1.9) reads:

$$E[n] = T[n] + V_{e,e}[n] + \int \mathrm{d}\mathbf{r} V_{ext} n(\mathbf{r}). \tag{1.15}$$

If we *define* the exchange-correlation energy as

$$E_{xc}[n] = E[n] - T_{ni}[n] - E_H[n] - \int d\mathbf{r} V_{ext} n(\mathbf{r}), \tag{1.16}$$

where $E_H[n]$ is the Hartree energy

$$E_H[n] = \frac{1}{2}\int\int \mathrm{d}\mathbf{r}\mathrm{d}\mathbf{r}' \frac{n(\mathbf{r})n(\mathbf{r}')}{|\mathbf{r}-\mathbf{r}'|}, \tag{1.17}$$

$E[n]$ takes the form, just by addition and substraction, of:

$$E[n] = T_{ni}[n] + E_H[n] + E_{xc}[n] + \int \mathrm{d}\mathbf{r} V_{ext} n(\mathbf{r}). \tag{1.18}$$

The Hartree energy in (1.17) captures the classical part of the Coulomb interaction between electrons and, to our benefit, is the biggest of the contributions of the internal potential energy. We take advantage of the fact that it has an explicit form as a density functional to separate its contribution[3]. Everything that is unknown is put into the exchange-correlation energy. Note that $T_{ni}[n]$ has been separated, because if the single-particle orbital picture is retained, it can be treated as before. $E_{xc}[n]$ is the big unknown in DFT. If it were known all many-electron problems could be solved exactly. Not

[3]Note that a self-interaction energy has been added in order to be able to write it as a density functional: according to (1.17)each electron would interact with itself, and in principle, the exchange-correlation energy should suppress this effect.

everything is lost, though: the smallness of this term compared to the rest of the terms in (1.18) makes it feasible to pursue an approximative approach[4].

Once $E[n]$ has been rewritten as in (1.18), we proceed to minimize it with respect to n and get the analog of (1.11) for the interacting case:

$$\frac{\delta}{\delta n(\mathbf{r})}\left(E[n]-\mu\int d\mathbf{r}n(\mathbf{r})\right)=\frac{\delta T_{ni}[n]}{\delta n(\mathbf{r})}+V_{ext}(\mathbf{r})+\int d\mathbf{r}'\frac{n(\mathbf{r}')}{|\mathbf{r}-\mathbf{r}'|}+\frac{\delta E_{xc}}{\delta n(\mathbf{r})}-\mu=0. \quad (1.19)$$

If we compare (1.11) and (1.19) we may identify

$$V_{ni}(\mathbf{r})\longleftrightarrow V_{ext}(\mathbf{r})+\int d\mathbf{r}'\frac{n(\mathbf{r}')}{|\mathbf{r}-\mathbf{r}'|}+\frac{\delta E_{xc}[n]}{\delta n(\mathbf{r})}\equiv V_{KS}[n](\mathbf{r}). \quad (1.20)$$

Once this identification has been made, the ground state density of the interacting system, is obtained by solving the single-particle Schrödinger equation

$$\left(-\frac{\hbar^2}{2m_e}\nabla^2+V_{KS}(\mathbf{r})\right)\phi_j(\mathbf{r})=\epsilon_j\phi_j(\mathbf{r}) \quad (1.21)$$

and constructing the density as in (1.14). The change with respect to the noninteracting case is that the potential now depends on the electronic density, so the equation has to be solved self-consistently, as we shall explain below (see Fig. 1.1).

It should be pointed out that DFT is formally exact, but the lack of knowledge of the $E_{xc}[n]$ functional makes it necessary to approximate it. The following section will briefly summarize the approximation we have used, the Local Density Approximation (LDA).

The Local Density Approximation

The Local Density Approximation (LDA) lies on the assumption that E_{xc} is a functional of the density n at each point of space. LDA expresses the E_{xc} of an inhomogeneous system as the integral over the exchange-correlation energy density of a homogeneous electron gas (HEG) evaluated at the local density:

$$E_{xc}^{LDA}[n]=\int d\mathbf{r}n(\mathbf{r})\epsilon_{xc}^{HEG}[n(\mathbf{r})]. \quad (1.22)$$

$\epsilon_{xc}^{HEG}[n(\mathbf{r})]$ is parametrized as follows [15]:

$$\epsilon_{xc}^{LDA}[n(\mathbf{r})]=\epsilon_x^{HEG}[n(\mathbf{r})]+\epsilon_c^{HEG}[n(\mathbf{r})], \quad (1.23)$$

[4]Nevertheless, it turns out that E_{xc} contributes significantly to the binding energy of matter, so finding good approximations is extremely important.

where ϵ_x^{HEG} has the analytical form [16]:

$$\epsilon_x^{HEG}[n(\mathbf{r})] = -\frac{3}{4}\left(\frac{3}{\pi}\right)^{1/3} n^{1/3}. \tag{1.24}$$

Still, there is no general analytical expression for ϵ_c^{HEG}, except for the high and low density limits, and these limiting values are combined with Monte Carlo simulations for the intermediate values of the density, giving rise to various parametrizations. The parametrization we have used is Perdew-Wang [17]:

$$\epsilon_x = -2c_0(1+\alpha_1 r_s)\ln\left(1+\frac{1}{2c_0\left(\beta_1 r_s^{1/2}+\beta_2 r_s+\beta_3 r_s^{3/2}+\beta_4 r_s^2\right)}\right), \tag{1.25}$$

where $r_s = \left(\frac{3}{4\pi n}\right)^{1/3}$ and c_0, β_1, β_2, β_3 and β_4 are got from Monte Carlo calculations.

Let us finally say that LDA suffers from certain general pathologies, namely the overestimation of binding energy, implying shorter bonds between atoms. The results are better for systems that resemble the HEG, but overall results are acceptable.

1.3 Method for electronic calculations

We use the software *Quantum Espresso* [18], which uses a plane wave basis to solve the Kohn-Sham equations (1.21) and takes advantage of Bloch's theorem.

1.3.1 Bloch's theorem and the plane wave basis

An ideal crystalline solid is a periodic structure with a period given by its unit cell. This makes $V_{KS}(\mathbf{r})$ to be periodic as well:

$$V_{KS}(\mathbf{r}) = V_{KS}(\mathbf{r}+\mathbf{T}) \tag{1.26}$$

with $\mathbf{T}$ any lattice vector. Any lattice vector can be written as a linear combination with integer coefficients of the basis vectors $\mathbf{a}_1$, $\mathbf{a}_2$ and $\mathbf{a}_3$: $\mathbf{T} = m_1\mathbf{a}_1 + m_2\mathbf{a}_2 + m_3\mathbf{a}_3$.

Bloch's theorem states that the eigenstates of the Hamiltonian of a single electron subject to a periodic potential as (1.26) can be chosen to be of the form [15]:

$$\begin{aligned} &\phi_{n\mathbf{k}}(\mathbf{r}) = e^{i\mathbf{k}\cdot\mathbf{r}}u_{n\mathbf{k}}(\mathbf{r}) \\ &\qquad\text{with} \\ &u_{n\mathbf{k}}(\mathbf{r}+\mathbf{T}) = u_{n\mathbf{k}}(\mathbf{r}). \end{aligned} \tag{1.27}$$

Here n denotes the band number and $\mathbf{k}$ is a wave vector laying in the first Brillouin zone (1ZB). $\mathbf{k}$ is restricted to the following values when Born-von Karman (periodic) boundary conditions are imposed ($\phi_{n\mathbf{k}}(\mathbf{r}+\mathbf{T}) = \phi_{n\mathbf{k}}(\mathbf{r})$):

$$\mathbf{k} = \sum_{i}^{3} \frac{m_i}{N_i}\mathbf{b}_i, \tag{1.28}$$

where N_i is the number of unit cells in the i^{th} direction[5], $\mathbf{b}_i$ are the reciprocal lattice basis vectors and $m_i \in [1, N_i]$.

The Fourier series expansion of the periodic potential (with period $\mathbf{T}$) only contains $\mathbf{k}$'s that are reciprocal lattice vectors $\mathbf{G}$[6]. When a plane wave basis is used, the Hamiltonian is block-diagonal: the potential only couples plane waves whose $\mathbf{k}$'s differ in a reciprocal lattice vector $\mathbf{G}$. Each block corresponding to a $\mathbf{k}$-point is a square matrix with as much columns (and rows) as the number of $\mathbf{G}$ vectors, which for an infinite solid is infinite. The eigenstates can be written as

$$\phi_{n\mathbf{k}}(\mathbf{r}) = \frac{1}{\sqrt{V}} \sum_{\mathbf{G}} c^{(n)}_{\mathbf{k}\text{-}\mathbf{G}} e^{i(\mathbf{k}\text{-}\mathbf{G})\cdot\mathbf{r}}, \tag{1.29}$$

where we see that only $\mathbf{k}$'s that differ in a reciprocal lattice vector are coupled. These eigenstates are readily proven to be of the form (1.27).

Following these arguments, one should in principle diagonalize the Hamiltonian in every $\mathbf{k}$ point in the 1BZ, but in practice the diagonalization is made in a mesh of $\mathbf{k}$-points, which has to be big enough to ensure convergence of the physical properties we are interested in. Plus, in (1.29) the sum runs over all $\mathbf{G}$ vectors. This sum has to be truncated for practical reasons and a cutoff energy E_{cut} is defined for this purpose:

$$\frac{\hbar^2}{2m_e} \mid \mathbf{k}+\mathbf{G} \mid^2 < E_{cut} \tag{1.30}$$

so that only $\mathbf{G}$'s satisfying this inequality are taken into account.

Pseudopotentials

Bloch functions tend to be very oscillating close to the nuclei, where the potential is strong. In this region, they cannot be described unless a huge cutoff energy is chosen, but this would be computationally very expensive. Instead, pseudopotentials are used.

[5] $N_i \sim N_A$.

[6] The definition of reciprocal lattice vectors is $e^{i\mathbf{G}\cdot\mathbf{T}} = 1$. Any reciprocal lattice vector can be written as $\mathbf{G} = m_1\mathbf{b}_1 + m_2\mathbf{b}_2 + m_3\mathbf{b}_3$, where $\mathbf{b}_1$, $\mathbf{b}_2$ and $\mathbf{b}_3$ are reciprocal lattice basis vectors.

A pseudopotential is an appropiate form for the $V_{e,I}$ external potential such that the wave functions do not oscillate in the proximity of the ion cores. Around each ion, the wave function reproduces the physical result outside a certain cutoff radius, but inside it, the wave function is not meaningful and is a mere artifact. We assume that this change in the wave functions inside those cutoff radii does not affect the description of our solid. Pseudopotentials pick the number of valence electrons that have to be taken into account in the calculations: the rest of the electrons are part of the core and move with the cations. In our case of study, the pseudopotential is not of a great interest, as we are dealing with a single-electron atom.

1.3.2 Calculation process. Self-consistency

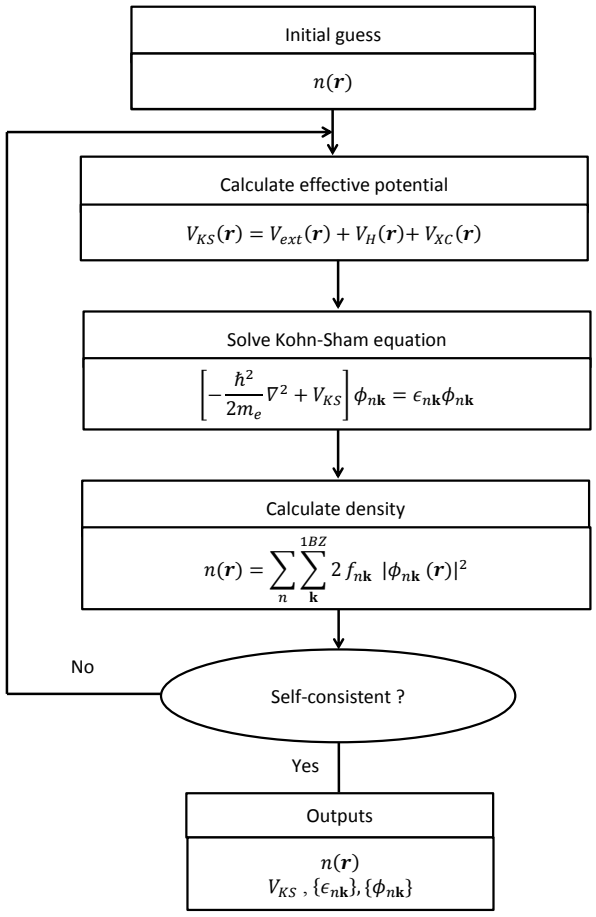

Figure 1.1: Selfconsistent loop for solving the Kohn-Sham equations. The subscript j becomes $n, \mathbf{k}$ when Bloch's theorem is used: each single-particle state is now identified by a $\mathbf{k}$ in the 1BZ and a band index n.

The steps followed by the *pw.x* package in *Quantum Espresso* to solve the Kohn-Sham equations are sketched in Fig. (1.1). First of all, an initial guess is made for the density, typically a superposition of atomic densities, out of which the first estimate of $V_{KS}[n]$ (1.20) is calculated. Then the Kohn-Sham equations (1.21) are solved in a plane-wave basis for the selected mesh of **k**-points. Note the change in the notation: $\epsilon_j \rightarrow \epsilon_{n\mathbf{k}}$, the eigenvalues of the Kohn-Sham Hamiltonian are now identified by the band index n and the wave vector **k**. Once the single-particle orbitals are known, the new density is calculated using (1.14) and is compared to the input density. With the notation of Bloch functions $\phi_{n\mathbf{k}}$, the density is calculated as:

$$n(\mathbf{r}) = \sum_{n} \sum_{\mathbf{k}}^{1BZ} 2 f_{n\mathbf{k}} |\phi_{n\mathbf{k}}(\mathbf{r})|^2 \tag{1.31}$$

where the occupation of the states is given by the Fermi-Dirac distribution $f_{n\mathbf{k}}$ and the factor 2 is due to the spin degeneracy of the Kohn-Sham states.

The loop is continued until selfconsistency is reached, using the output density to recalculate $V_{KS}[n]$ for the next step. We say that the solution is selfconsistent when the total energy does not vary beyond a desired threshold from one iteration to another.

1.4 Ionic motion

So far we have only paid attention to the electronic part of our problem, which has been properly separated from the ionic degrees of freedom using the Born-Oppenheimer approximation introduced in section (1.1). Electronic degrees of freedom are, nonetheless, insufficient for the description of many phenomena such as the observed specific heat of the solids, or superconductivity, which arises from the electron-phonon coupling. To account for these phenomena, ionic degrees of freedom have to be included in the analysis.

As stated in (1.6) and (1.7) the Schrödinger equation for the ions does depend on the electronic solution and is thus necessary to first solve the electronic problem. From (1.7) we see that the ionic potential is $U(\mathbf{R}_1, ..., \mathbf{R}_M) \equiv V_{I,I} + E_e(\mathbf{R}_1, ..., \mathbf{R}_M)$. The ionic positions are not fixed anymore. Ions oscillate around their equilibrium lattice sites so that the position of the s^{th} ion in the n^{th} unit cell is

$$\mathbf{R}_{ns} = \mathbf{T}_n + \boldsymbol{\tau}_s + \mathbf{u}_{ns}, \tag{1.32}$$

where $\mathbf{T}_n$ is a lattice vector (from the origin to the origin of the n^{th} cell), $\boldsymbol{\tau}_s$ is a basis vector that denotes the position of the s^{th} atom inside the n^{th} cell and $\mathbf{u}_{ns}$ is the displacement of this atom from the equilibrium position. When displacements are much

smaller than the interatomic distance, a low-order Taylor expansion of the potential is a valid approximation.

1.4.1 The harmonic approximation

The first approximation is made retaining only terms up to second order in the displacements [19]:

$$U = U_0 + \sum_{ns\alpha} \Phi_s^{\alpha}(\mathbf{T}_n) u_s^{\alpha}(\mathbf{T}_n) + \frac{1}{2} \sum_{ns\alpha} \sum_{n's'\alpha'} \Phi_{ss'}^{\alpha\alpha'}(\mathbf{T}_n, \mathbf{T}_{n'}) u_s^{\alpha}(\mathbf{T}_n) u_{s'}^{\alpha'}(\mathbf{T}_{n'}), \tag{1.33}$$

where $\Phi_s^{\alpha}(\mathbf{T}_n) \equiv \frac{\partial U}{\partial u_s^{\alpha}(\mathbf{T}_n)}\Big|_{eq}$ is identically zero by definition of the equilibrium and

$$\Phi_{ss'}^{\alpha\alpha'}(\mathbf{T}_n, \mathbf{T}_{n'}) \equiv \frac{\partial^2 U}{\partial u_s^{\alpha}(\mathbf{T}_n) \partial u_{s'}^{\alpha'}(\mathbf{T}_{n'})}\Big|_{eq} \tag{1.34}$$

are the atomic force constants. α and α' are labels for the cartesian coordinates x, y and z. The U_0 term in (1.33) yields the ground state energy of the crystal including the ion-ion contribution and the first order term is zero. The classical equations of motion

$$m_s \ddot{u}_s^{\alpha}(\mathbf{T}_n) = \sum_{n's'\alpha'} \Phi_{ss'}^{\alpha\alpha'}(\mathbf{T}_n, \mathbf{T}_{n'}) u_{s'}^{\alpha'}(\mathbf{T}_{n'}) \tag{1.35}$$

can be solved if we seek a solution of the form

$$u_s^{\alpha}(\mathbf{T}_n) = \epsilon_s^{\alpha}(\mathbf{q}) e^{[i(\mathbf{q}\cdot(\mathbf{T}_n + \boldsymbol{\tau}_s) - \omega(\mathbf{q}))]}. \tag{1.36}$$

The problem is thus reduced to the diagonalization of the dynamical matrix

$$D_{ss'}^{\alpha\alpha'}(\mathbf{q}) = \sum_{n} e^{-i\mathbf{q}\cdot(\mathbf{T}_n + \boldsymbol{\tau}_s - \mathbf{T}_{n'} - \boldsymbol{\tau}_{s'})} \Phi_{ss'}^{\alpha\alpha'}(\mathbf{T}_n, \mathbf{T}_{n'}), \tag{1.37}$$

so that the normal modes with frequency $\omega_\nu(\mathbf{q})$ and polarization vector $\boldsymbol{\epsilon}_{s\nu}(\mathbf{q})$ are found by solving

$$\omega_\nu^2(\mathbf{q}) \epsilon_{s\nu}^{\alpha}(\mathbf{q}) = \sum_{s'\alpha'} \frac{D_{ss'}^{\alpha\alpha'}(\mathbf{q})}{\sqrt{m_s m_{s'}}} \epsilon_{s'\nu}^{\alpha'}(\mathbf{q}). \tag{1.38}$$

Here ν is the branch index (there are as many branches as degrees of freedom in a unit cell, *i.e.*, three times the number of atoms per unit cell), and $\mathbf{q}$ is a wave-vector in the

1BZ (there are as many $\mathbf{q}$'s as unit cells in the crystal). In total, there are as many normal modes as degrees of freedom in the whole crystal, as expected.

In classical mechanics, solving (1.38) gives the normal modes of the ions. When these normal modes are quantized, independent harmonic oscillators arise. As it is known from quantum mechanics, the eigenvalues of an harmonic oscillator corresponding to the branch ν and with wave vector $\mathbf{q}$ are $E_{\nu\mathbf{q}} = (\frac{1}{2} + n_{\nu\mathbf{q}})\hbar\omega_\nu(\mathbf{q})$. The equivalence between normal modes and phonons is the following: a harmonic oscillator corresponding to a mode identified by a given ν and $\mathbf{q}$ that is in the n^{th} excited state is equivalent to having n phonons of that mode.

For a numerical treatment of the problem we use Density Functional Perturbation Theory (DFPT) as implemented in the *ph.x* package in *Quantum Espresso*. For this purpose we need second order derivatives of U with respect to the ionic positions. Using the chain rule, most of the expressions that appear in these derivatives are analytical, we only need to calculate the first derivative of the density with respect to the ionic positions. To get it, first order perturbation theory is used (linear response). The calculation has to be done self-consistently and is computationally demanding [20].

1.5 Anharmonicity

The harmonic approximation does not account for several phenomena as thermal expansion of the solids or finite thermal conductivity, and it cannot explain the temperature dependence of the phonon frequencies either. The breakdown of the harmonic approximation happens when the ionic displacements with respect to the equilibrium positions cannot be considered small anymore, and thus one is forced to include terms beyond the quadratic displacements for a correct description of the potential. This can be the case when the temperature is high or the atoms present in the crystal are very light, as is our case. When this happens, anharmonicity has to be taken into account.

Anharmonicity can be treated perturbatively, but perturbation theory is only valid in the regime where the harmonic potential is much larger than higher-order terms. When higher-order terms are as important as the second-order term, a nonperturbative method is desirable. The self-consistent harmonic approximation (SCHA) [22] is one of such methods, and is variational instead of perturbative. Our work is based on a stochastic implementation of the SCHA, the so-called stochastic self-consistent harmonic approximation (SSCHA)[11].

1.5.1 The stochastic self-consistent harmonic approximation (SSCHA)

In the SSCHA the free energy of the system is minimized with respect to the phonon frequencies, polarization vectors and ionic equilibrium positions. Given the ionic Hamil-

tonian $H = T_I + U$ in (1.7), the partition function is $Z_H = \mathrm{tr}\left[e^{-\beta H}\right]$ and the Helmholtz free energy is:

$$F_H = -\frac{1}{\beta}\ln Z_H = \mathrm{tr}\left(\rho_H H\right) + \frac{1}{\beta}\mathrm{tr}\left(\rho_H \ln \rho_H\right), \tag{1.39}$$

where ρ_H is the density matrix and $\beta = \frac{1}{k_B T}$.

A variational principle may be stablished for the free energy. For any trial $\rho_{\mathcal{H}}$ the free energy $\mathcal{F}_H(\mathcal{H}) = \mathrm{tr}\left(\rho_{\mathcal{H}} H\right) + \frac{1}{\beta}\mathrm{tr}\left(\rho_{\mathcal{H}} \ln \rho_{\mathcal{H}}\right)$ satisfies the Gibbs-Bogoliubov inequality

$$F_H \leq \mathcal{F}_H(\mathcal{H}). \tag{1.40}$$

We can also define $F_{\mathcal{H}} = \mathrm{tr}\left(\rho_{\mathcal{H}}\mathcal{H}\right) + \frac{1}{\beta}\mathrm{tr}\left(\rho_{\mathcal{H}} \ln \rho_{\mathcal{H}}\right)$, which is the exact free energy that corresponds to a Hamiltonian $\mathcal{H}$. By addition and substraction of $\mathrm{tr}\left(\rho_{\mathcal{H}}\mathcal{H}\right)$ we get

$$\mathcal{F}_H(\mathcal{H}) = F_{\mathcal{H}} + \mathrm{tr}\left[\rho_{\mathcal{H}}\left(U - \mathcal{U}\right)\right], \tag{1.41}$$

which is the function that has to be minimized with respect to a trial Hamiltonian $\mathcal{H}$.

In the SSCHA the trial potential $\mathcal{U}$ of the trial Hamiltonian $\mathcal{H}$ is restricted to a harmonic one, so $\mathcal{H}$ takes the form:

$$\mathcal{H} = \sum_s \sum_\alpha \frac{\left(P_s^\alpha\right)^2}{2m_s} + \frac{1}{2}\sum_{ss'}\sum_{\alpha\alpha'} u_s^\alpha \widetilde{\Phi}_{ss'}^{\alpha\alpha'} u_{s'}^{\alpha'} \tag{1.42}$$

with the advantage that the term $F_{\mathcal{H}}$ in (1.41) and the density matrix $\rho_{\mathcal{H}}$ can be expressed in a closed form in terms of the phonon frequencies and polarizations, which facilitates the calculations.

At this point it should be stressed that the trial force-constants matrix $\widetilde{\Phi}_{ss'}^{\alpha\alpha'}$ is not necessarily (and will not in general be) the same as the force-constants matrix $\Phi_{ss'}^{\alpha\alpha'}$ associated to the second order term in the Taylor expansion of the ionic potential U (see Eq (1.34)); it is the one that minimizes $\mathcal{F}_H(\mathcal{H})$. A simple analogy might be helpful here. Suppose that we have the black curve in Fig. 1.2 and we want to fit a harmonic function to it. If the Taylor expansion around the minimum is truncated in the second order, we have the red curve. So as to speak, this is what the harmonic approximation does. However, even if the profile we have drawn is clearly not harmonic, if we try to find the best harmonic fit, it turns out to be the blue curve, which is shifted to the right. This is an oversimplification of what SSCHA does, because for SSCHA not all the points have the same importance: they are weighted by the density matrix. However, this intuitive idea may help.

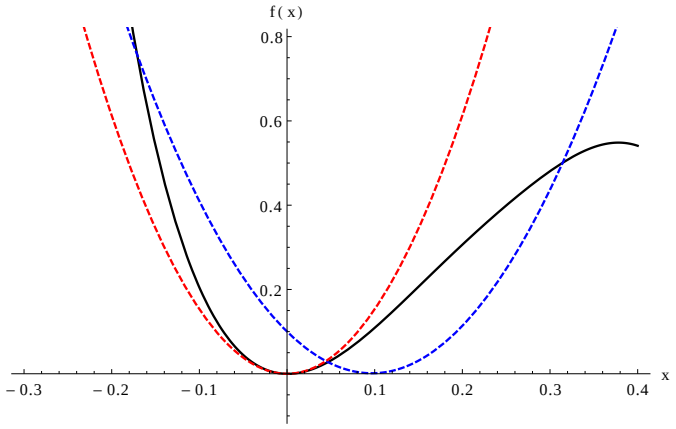

Figure 1.2: Analogy of the idea behind SSCHA. The actual curve is the black (full) one, the fitting around the minimum is the red (dashed) one and the best harmonic fitting to all the curve is the blue (dotted) line.

$\mathcal{F}_H(\mathcal{H})$ is to be minimized with respect to $\widetilde{\Phi}$ but also with respect to $\mathbf{R}_{eq}$, the equilibrium positions of the ions[7]. The minimization is carried out in a subspace of the parameters that preserves crystal symmetries: $\widetilde{\Phi}$ and $\mathbf{R}_{eq}$ are written on a symmetrized vector basis and what are minimized are the coefficients of such basis vectors. We call N_p the number of independent coefficients. The minimization is perfomed using a conjugate-gradient method. The expressions for $\mathcal{F}_H(\mathcal{H})$ and its gradients are as follows:

$$\mathcal{F}_H(\mathcal{H}) = F_{\mathcal{H}} + \int \mathrm{d}\mathbf{R}\,[U(\mathbf{R}) - \mathcal{U}(\mathbf{R})]\,\rho_{\mathcal{H}}(\mathbf{R}) \tag{1.43}$$

$$\nabla_{\mathbf{R}_{eq}}\mathcal{F}_H(\mathcal{H}) = -\int \mathrm{d}\mathbf{R}\,[\mathbf{f}(\mathbf{R}) - \mathbf{f}_{\mathcal{H}}(\mathbf{R})]\,\rho_{\mathcal{H}}(\mathbf{R}) \tag{1.44}$$

$$\begin{aligned}\boldsymbol{\nabla}_{\widetilde{\Phi}}\mathcal{F}_H(\mathcal{H}) = &-\sum_{ss'\alpha\alpha'\nu}\sqrt{\frac{m_{s'}}{m_s}}(\epsilon^{\alpha}_{s\nu\mathcal{H}}\boldsymbol{\nabla}_{\widetilde{\Phi}}\ln a_{\nu\mathcal{H}} + \boldsymbol{\nabla}_{\widetilde{\Phi}}\epsilon^{\alpha}_{s\nu\mathcal{H}})\epsilon^{\alpha'}_{s'\nu\mathcal{H}} \\ &\times\int \mathrm{d}\mathbf{R}[f^{\alpha}_{s}(\mathbf{R}) - f^{\alpha}_{s\mathcal{H}}(\mathbf{R})](R^{\alpha'}_{s'} - R^{\alpha'}_{s'\mathrm{eq}})\rho_{\mathcal{H}}(\mathbf{R}).\end{aligned} \tag{1.45}$$

In these expressions $\mathbf{R} \equiv \{\mathbf{R}_1, ...\mathbf{R}_M\}$ is a general ionic configuration. $\rho_{\mathcal{H}}(\mathbf{R})$ is the probability to find the system described by $\mathcal{H}$ in a general ionic configuration $\mathbf{R}$, which in normal coordinates is a product of gaussians. $a_{\nu\mathcal{H}} = \sqrt{\hbar\coth(\beta\hbar\omega_{\nu(\mathcal{H})}/2)(2\omega_{\nu(\mathcal{H})})}$ is called the normal length[8] of mode ν and is the standard deviation of the gaussians.

[7] Implicitly, it is minimized with respect to phonon frequencies and polarizations, as the diagonalization of the force constant matrices $\widetilde{\Phi}$ gives rise to $\omega_{\nu(\mathcal{H})}$and $\epsilon^{\alpha}_{s\nu(\mathcal{H})}$.

[8] Even if it has dimensions of length times square root of mass.

Finally, $\mathbf{f}(\mathbf{R})$ is the vector formed by all the atomic forces for the ionic configuration $\mathbf{R}$ and $\mathbf{f}_{\mathcal{H}}(\mathbf{R})$ are the harmonic forces. The only nonanalytic terms in equations (1.43) - (1.45) are the integrals. The usual approach for their evaluation involves the calculation of higher order $\Phi^{\alpha,\alpha',\ldots,\alpha^{(n)}}_{s,s',\ldots,s^{(n)}}$ coefficients, which is a difficult task. In the SSCHA method, however, these integrals are evaluated stochastically. To calculate the gradient, we therefore need to calculate the forces $\mathbf{f}(\mathbf{R})$.

For the stochastic evaluation we use the relationship

$$\int d\mathbf{R}\mathcal{O}(\mathbf{R})\rho(\mathbf{R}) \simeq \frac{1}{N_c}\sum_{I=1}^{N_c}\mathcal{O}(\mathbf{R}_I) \equiv \langle\mathcal{O}\rangle, \tag{1.46}$$

where the set of $\mathbf{R}_I$ configurations is created according to the distribution $\rho(\mathbf{R})$. $\mathcal{O}$ is any operator and N_c is the number of configurations. The expression is exact in the limit of $N_c \to \infty$. Being an stochastic procedure, there always exists a statistical error, which scales as $1/\sqrt{N_c}$.

The calculation flowchart in Fig. 1.3 summarizes the minimization process. An initial guess $\mathcal{H}_{j_0}$ (in the first step $j_0 = 0$) is made for the trial Hamiltonian. This trial Hamiltonian is used to create N_c ionic configurations according to $\rho_{\mathcal{H}_j 0}(\mathbf{R})$. The energy and atomic forces in each of the configurations are calculated in supercells because, when the atomic force constant matrices are calculated in supercells, the Fourier transform provides the dynamical matrices in a $\mathbf{q}$-mesh of the same size as the supercell. These calculations are performed using the *pw.x* package in *Quantum Espresso*. The obtained data are used to evaluate the integrals in (1.43) - (1.45). Then a conjugate gradient step is made, and the $\mathbf{R}_{eq}$ and $\widetilde{\Phi}$ parameters are updated so a new $\mathcal{H}_j$ is got.

At this point, new configurations should be created, following $\rho_{\mathcal{H}_j}$. However, this would be very inefficient as it would imply the calculation in supercells again. What is done instead is to use a reweighting technique, and as long as $\langle\frac{\rho_{\mathcal{H}_j}}{\rho_{\mathcal{H}_{j_0}}}\rangle$ does not deviate substantially from unity, the configurations created with $\mathcal{H}_{j_0}$ can be reused[9]. If the deviation is larger than a fixed parameter η new configurations have to be created out of $\mathcal{H}_j$.

Otherwise, when a coefficient satisfies one of the following conditions:

(a) the coefficient has a gradient smaller than a fixed convergence criterium or

(b) the error is bigger than the value of the coefficient,

this coefficient is kept fixed in the subsequent conjugate gradient steps. When all the coefficients satisfy either (a) or (b) the minimization stops. One can always add extra

[9]We have a correction to (1.46): $\int d\mathbf{R}\mathcal{O}(\mathbf{R})\rho(\mathbf{R}) \simeq \frac{1}{N_c}\sum_{I=1}^{N_c}\mathcal{O}(\mathbf{R}_I)\frac{\rho_{\mathcal{H}_j}}{\rho_{\mathcal{H}_{j_0}}}$ which is still accurate in the condition mentioned above is satisfied.

configurations to reduce the statistical error and acquire the desired precision [10].

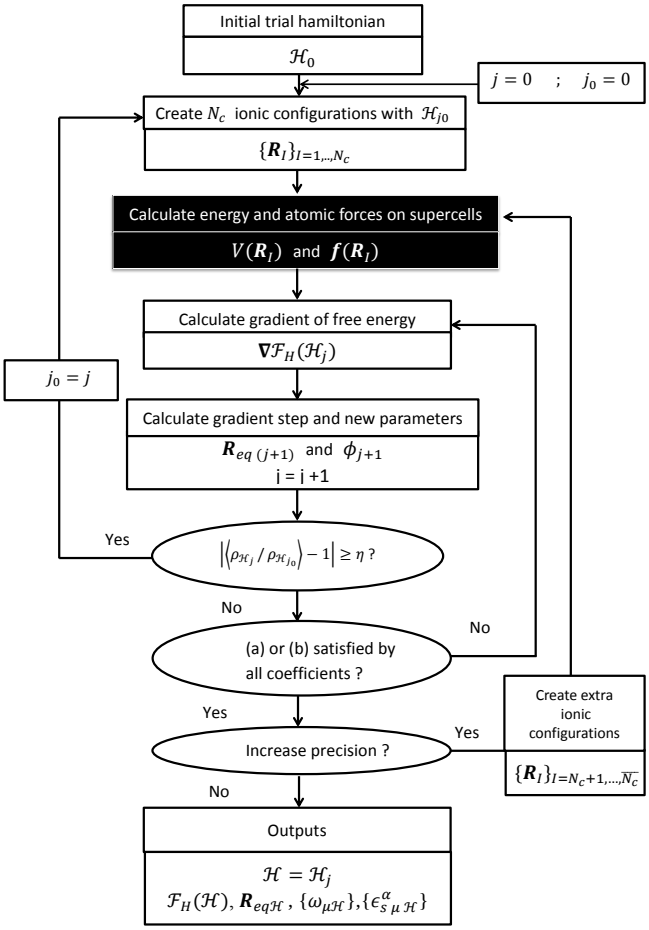

Figure 1.3: Calculation flowchart for the SSCHA. The step marked in black, the calculation of forces in supercells, is the most time-demanding, and the program is optimized to call it as little as possible.

[10] *i.e.*, to reduce the number of coefficients that satisfy (b) and increase the ones that satisfy (a).

Chapter 2

Results and discussion

2.1 The Cmca-4 structure: relaxing the structure

The system we consider is *Cmca*-4 hydrogen under a pressure of 414 GPa and at T=0 K. This structure has been found to be metallic, and stable at pressures in the range 385-490 GPa [8], so we pick an intermediate value to perform the analysis.

The crystal structure consists of a base centered orthorhombic conventional unit cell, with atoms in $8f$ Wyckoff positions. To find the cell parameters and the equilibrium positions of the atoms at the pressure we are interested in, which is crucial to have a good description of the electronic and vibrational properties of the system, the crystal structure has to be relaxed. We use the 'vc-relax' tool from the *pw.x* package in *Quantum Espresso*. The program performs an iterative process to minimize the forces between atoms and changes the cell parameters in order to reach the inposed target pressure. Initial atomic position and cell parameters have been taken from the supplementary material of Ref. [8], which provides these data at 300 GPa. In this process, the convergence threshold for the atomic forces was set to 10^{-4}Ry/a.u. [1], as values of the forces below that are necessary for a good accuracy in phonon calculations.

As we are dealing with a metallic solid and the mesh of **k**-points is finite in practice (see Section 1.3.1), a new parameter has to be introduced in the calculations, the so-called smearing. This numerical artifact creates a distribution of the occupation of the orbitals, as if the system were at a finite, nonzero, temperature. This is useful because as in a metal the Fermi level lies in a half-filled band, at T=0 K the **k**-points that are occupied or unoccupied change abruptly. This is not problematic when the number of **k**-points is very large, as the grid is very dense and the points are very close to each other; however, when the mesh of **k**-points has been reduced for practical reasons, the points are more spaced and it is too drastic to keep some states near the Fermi level occupied, and some

[1] 1 Ry = 13.605 eV; 1 a.u. = 0.529 Å.

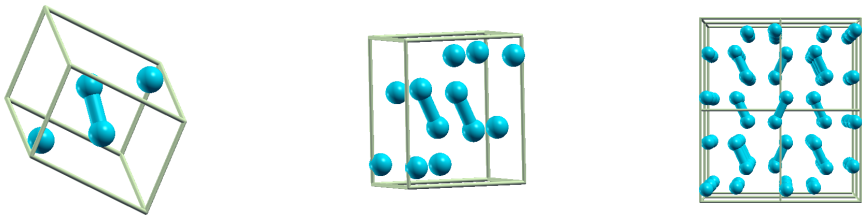

(a) (b) (c)

Figure 2.1: (a) Primitive cell of the *Cmca*-4 structure. There are 4 atoms per primitive cell. (b) Conventional unit cell. Base centered orthorhombic containing 8 atoms. (c) Projection of the structure on the YZ plane. The two types of dimers can be appreciated, tilted to left and right.

others unoccupied. The smearing parameter allows to weight the **k**-points around the Fermi level. At T=0 the occupation versus the energy should be a step function, but the broadening of the occupation can be controlled, and this is used to perform the integrals in the Brillouin zone. The smearing we have used is the Methfessel-Paxton one [21].

We have perfomed a study of the convergence of the E_{cut}, smearing broadening and number of **k**-points and we have found a convergence of 3 meV per atom for $E_{cut} = 65$ Ry, a broadening of 0.01 Ry and a $16 \times 16 \times 16$ mesh. We use exchange-correlation potentials within the local density approximation and a norm-conserving pseudopotential.

After relaxing the structure, the values of the cell parameters are found to be: $a = 1.553$ Å, $b = 2.718$ Å and $c = 2.367$ Å. Atoms are in Wyckoff positions $8f$ with fractional coordinates y = 0.368 and z = 0.430. The structure can be visualized in Fig. 2.1. In this structure dimers persist and we find that the intramolecular bond lenght is of 0.793 Å for both kind of molecules (tilted to the left and right in Fig. 2.1(c)).

2.2 Electronic band structure

Once the structure is relaxed, we proceed to calculate the band structure of the solid. At this point it should be noted that the eigenvalues of the Kohn-Sham orbitals (the solutions of (1.21)) are the energies of a ficticious noninteracting system, and in principle cannot be adscribed to the energies of the electrons. There is quite a lot of literature that treats this issue but given the agreement of these eigenvalues and the experimentally measured band structures, these eigenvalues are taken to be equal to the electronic energies. This hypothesis being made, the Kohn-Sham equations have to be solved self-consistently for the **k** points in the above mentioned $16 \times 16 \times 16$ mesh. When V_{KS} is known, a non self-consistent calculation can be performed along a path of selected

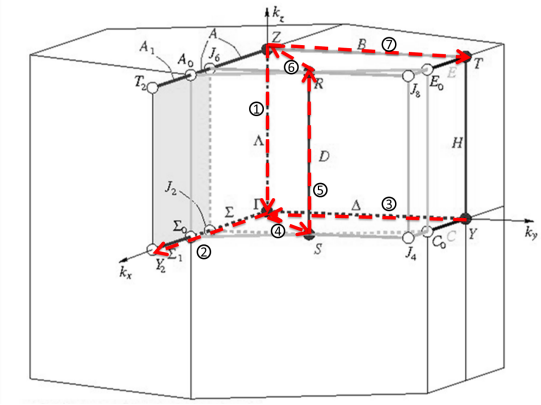

Figure 2.2: First Brillouin zone of space group *Cmca*-4 and high symmetry lines along which bands and phonon branches are plotted. The path is $Z-\Gamma$; $\Gamma-Y2$; $Y-\Gamma$; $\Gamma-S$; $S-R$; $R-Z$; $Z-T$. Y2 and Y are equivalent points, so the jump is justified.

k-points, usually the high symmetry lines of the Brillouin zone. The selected path for the representation of the bands (and later on for the phonons) is displayed in Fig. 2.2.

Fig. 2.3 shows the bands along the selected path. The Fermi level, the highest occupied energy, is set to zero. We can see that the material is metallic, as bands cross the Fermi level in the $\Gamma - Y$ line.

As the solid is formed by molecules we can interpret the bands starting from a picture of bonding and antibonding molecular orbitals in the two H_2 molecules. We would have intramolecular bonding and antibonding states, as well as intermolecular bonding and antibonding ones. The lowest band is the one correspondig to intramolecular and intermolecular bonding, and the second occupied band corresponds to intramolecular bonding, but intermolecular antibonding. Then, as energy goes up, we have the bands that correspond to intramolecular antibonding, but these are unoccupied.

2.3 Phonons

After the electronic bands have been calculated, we proceed to calculate the phonon spectrum of the *Cmca*-4 hydrogen at T=0 K. Even if in classical physics absolute zero implies no motion, in quantum physics this statement is incorrect. Due to Heisenberg's uncertainty principle, one cannot exactly determine the position of an ion and its momentum at the same time: the smaller the uncertainty is in the position, the bigger it is in the momentum, so there always exists, even at T=0 K, a zero point motion. To put it in another way, if the ionic positions were completely fixed, their wave function would be a Dirac delta and the uncertainty in the position would be zero; but this way, its Fourier transform, which gives the distribution of the values the momentum can take,

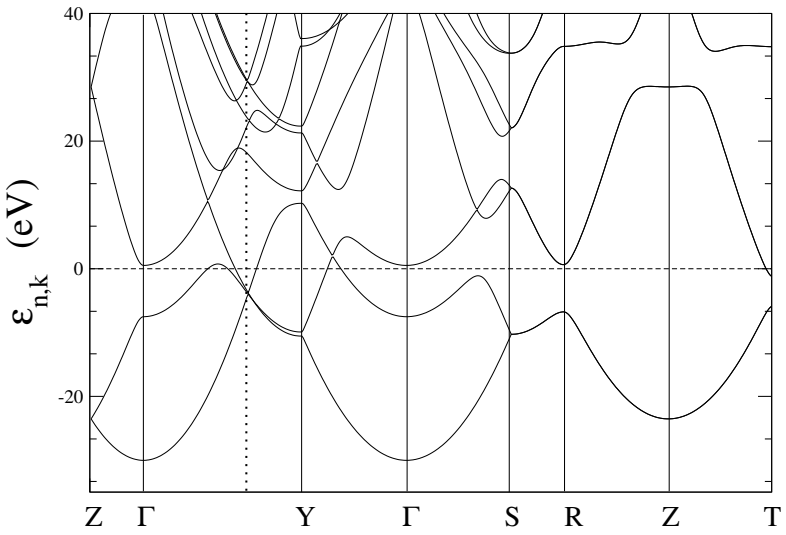

Figure 2.3: Electronic band structure.

would be constant, meaning that any value for the momentum is equally probable: the uncertainty in the momentum would be infinite.

When the ionic Hamiltonian in the harmonic approximation is written in normal coordinates, independent harmonic oscillators emerge (Section 1.4.1). What happens at T=0 K is that all these oscillators are in the ground state: all the normal modes have a zero point motion. Moreover, if even at absoute zero the displacements of the ions are considerably large, due to, for example, the lightness of the atoms implied, as in this case hydrogen, the harmonic approximation may not suffice to describe the system correctly.

First of all, we study the system with the harmonic approximation, using the density functional perturbation theory (DFPT) and we perform some extra analyses that show that a method that treats anharmonicity has to be included. Then, we apply the SSCHA and get the phonon dispersion that includes anharmonicity within this approximation, to draw some conclusions about the role of the anharmonic effects on *Cmca*-4 hydrogen.

2.3.1 Harmonic approximation

Following the procedure of section (1.4.1) and using the *ph.x* package in *Quantum Espresso*, we have calculated the harmonic phonon spectrum in the same path as the bands (Fig. 2.2). To do so, the software has to calculate the dynamical matrix in a mesh of **q**-points and diagonalize it in order to get the frequencies and polarization vec-

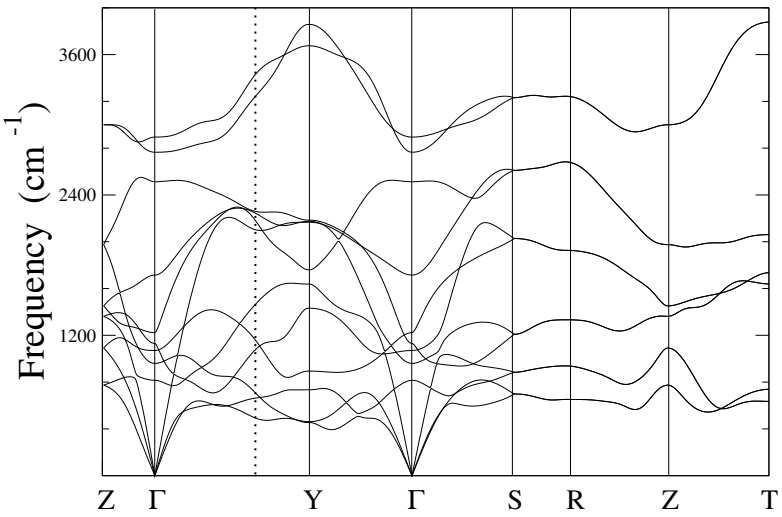

Figure 2.4: Phonon dispersion. Frequency in cm^{-1}; 1 cm^{-1} = 0.03 THz

tors. The size of the mesh used is $6 \times 6 \times 6$[2], which leads to 52 dynamical matrices that are independent once the symmetries of the crystal have been taken into account. Then an interpolation scheme is applied: force constant matrices in real space are got by Fourier-transforming the dynamical matrices and then dynamical matrices at new **q'** points are computed and diagonalized. This interpolation has been used to get the phonon frequencies along the path in Fig. 2.2.

In Fig. 2.4 twelve branches can be observed, corresponding to the three degrees of freedom of each of the four atoms in the primitive unit cell. Three of the branches, the acoustic ones, have a zero frequency at the Γ point and correspond to the three translational degrees of freedom of the crystal. The other nine are optical branches: the atoms within a primitive cell do not move together. At the Γ point all the cells move in the same way, at the rest of **q**-points there is a $e^{\mathbf{q}\cdot\mathbf{T}}$ phase factor between the cells. We can also see that two of the branches are on top of the others and never get crossed with them. As we shall see, these branches are the vibrons, and correspond to the vibrational modes of the molecules, where, as their binding is stronger, the frequency is higher. If there were no interaction between the molecules of different cells, there would be no dispersion in the branches, *i.e.*, they would be plane. However, the dispersion is quite big, so the molecules belonging to different cells interact substantially. This can be associated to an intramolecular binding that is not very tight. Plus, the fact that the vibrons are not mixed with the rest of the branches implies that the vibration modes of the molecules are independent from the rest of the ionic movements[3]. However, the

[2]This mesh is smaller than the one for electronic calculations, as calculating the dynamical matrices is computationally very demanding.

[3]When two modes are degenerate (have the same frequency), one can make linear combinations of the polarization vectors that are still eigenvectors of the dynamical matrix, so the movements are not independent anymore.

frequencies of the vibrons are not very high even if the pressure is as high as 414 GPa. This may seem counterintuitive, one could expect that increasing pressure would get the molecules closer and increase the vibration frequency. This is true, indeed, but only in a certain range of pressures. Starting from zero pressure, the frequency of the vibrons increases until we get to about 80 GPa. Then, it starts to go down. As we will see later, when anharmonicity is included, the frequency of the vibrons is lowered and they get mixed with lower branches.

2.3.2 Vibrational modes at the Γ point

To get a first intuition of the ionic motion we sketch the vibrational modes at the Γ point. The advantage of studying this point is that, as mentioned above, at Γ all unit cells move in phase: the displacement of an ion is the same as the displacement of the equivalent ion in the neighboring cell. *Quantum Espresso* returns us the polarization vectors of each mode, so we know how the atoms move for each of them inside the unit cell. In Fig. 2.5 we depict the ionic displacements of the 9 optical modes of the structure. It can be observed that in (b), (c), (d) and (f) the molecules rotate (rotons), in (a), (e) and (g) they move translationally and in (h) and (i), with the highest frequency, they vibrate (vibrons).

Energy profiles and harmonic frozen phonon calculation

Displacing the atoms according to the polarization vectors of each mode takes the system out of equilibrium. Consequently, its energy increases. We work at the Γ point still, where we only have to fix our attention in one primitive cell, as all the rest move in phase. We displace the atoms with different amplitudes according to the polarization vector of each mode and we calculate the energy of the primitive unit cell for each of the positions. The profiles have been plotted in Fig. 2.6.

We must stress that this approach only gives us information about the interaction of a mode with itself, but anharmonic effects also include the interaction between modes, so it should be clear that this kind of calculation only provides a first feeling. We observe that the profiles are not harmonic (although some of them deviate only slightly from the quadratic behavior) and, even if as warned this kind of calculation only takes into account the interaction of the mode with itself, it can already be seen that anharmonic effects may be important to describe the ionic motion of the system.

In the harmonic approximation modes are independent, so the frequency that the software *Quantum Espresso* has computed has to be compatible with the one extracted from the second order derivative around zero[4] of the energy profiles in Fig. 2.6. Table

[4] $m\omega^2 = k$, where k is the second derivative of the potential energy. We perform this derivative numerically: $k = \frac{U(x+h)-2U(x)+U(x-h)}{h^2}$.

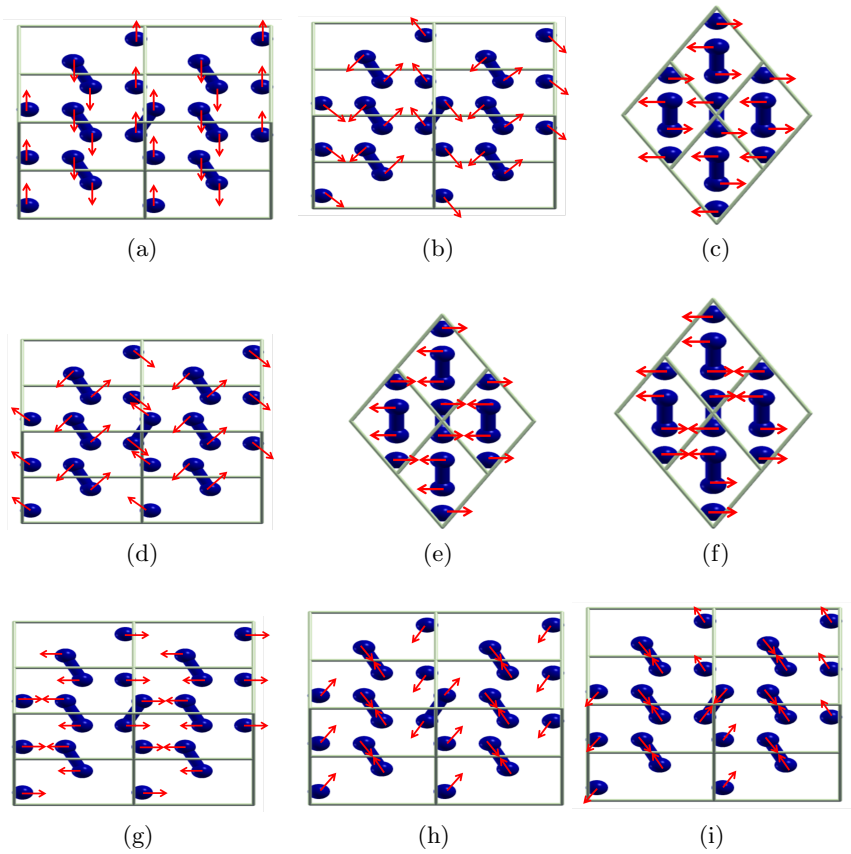

Figure 2.5: Displacement of the atoms at the point Γ according to the nine optical modes, in ascending order of frequency.

2.1 compares both of them. The two methods for calculating the phonon frequencies are valid but the procedure is completely different, hence the small differences in the frequencies, that come on the one hand from the finitness of the step h in the numerical derivative and on the other hand from the approximations made in the DFPT.

If we look at the forms of the profiles in Fig. 2.6, two of them, (b) and (i), are clearly non-symmetric. The latter is a vibron and the potential takes the form that is expected for an independent molecule. However, even if (h) also corresponds to a vibron, the profile is symmetric. This can be understood if we look at Fig. 2.5(h): here, the two types of molecules (the ones tilted to the left and the ones tilted to the right) move in opposite phase, when the molecules tilted to the left contract, the others expand, and vice versa. This produces a positive displacement and a negative one to be equivalent: when they are separating from a certain atom, they are at the same time getting close to another. This is not the case for the (i) vibron: here the two molecules move in phase so the potential is different when they are contracted or expanded, as their distance to

Mode (Fig. 2.6)	*Quantum Espresso* (QE)	2^{nd} deriv. profile (DP)	Difference (%)
(a)	24.55	24.45	-0.41
(b)	28.91	29.23	1.11
(c)	32.23	32.09	-0.43
(d)	34.04	34.46	1.23
(e)	36.80	36.64	-0.43
(f)	51.63	51.27	-0.70
(g)	75.64	75.75	0.15
(h)	83.23	83.17	-0.07
(i)	87.13	86.75	-0.44

Table 2.1: Comparison between the frequency obtained by *Quantum Espresso* (by means of DFPT) and the one obtained out of the 2^{nd} order derivative of the profile (harmonic frozen phonon, HFP), in THz. The last column is the relative difference $\frac{\mathrm{HFP-DFPT}}{\mathrm{DFPT}}$.

neighboring atoms varies.

The next thing we do is to solve numerically the Schrödinger equation for an ion subject to the fitted potential energies (a)-(i):

$$\left(-\frac{\hbar^2}{2m_H}\frac{\mathrm{d}^2}{\mathrm{d}(\Delta \mathrm{x})^2} + U(\Delta x)\right)\varphi(\Delta x) = \epsilon\varphi(\Delta x). \tag{2.1}$$

Here m_H is the mass of an hydrogen ion and $U(\Delta x)$ is the potential energy, a fitting of the curves (a)-(i) in Fig. 2.6. If the potential is harmonic, the energy quantum is constant (the eigenvalues equispaced). Nonetheless, when it is not harmonic, the distance between subsequent energies varies, so to define the phonon frequency we take the difference between the first excited state and the ground state, which is the transition that is measured in low temperature experiments. This value, together with the frequency computed within the harmonic approximation and the one obtained when applying the SSCHA can be seen in Table 2.2.

We can observe some features looking at the wave functions in Fig. 2.6. For instance, in the case of the non-symmetric wells the displacement of the wave function becomes evident. We compute the mean value of the displacement, $\langle \Delta x \rangle$ for the cases (b) and (i).

$$\int \mathrm{d}\,(\Delta x)\,\Delta x\left|\varphi_{anharm-(b)}\,(\Delta x)\right|^2 = -0.049\ \text{Å} \tag{2.2}$$

$$\int \mathrm{d}\,(\Delta x)\,\Delta x\left|\varphi_{anharm-(i)}\,(\Delta x)\right|^2 = \ 0.031\ \text{Å} \tag{2.3}$$

whereas in the harmonic case it is zero. Here we see that, apart from a change in the frequency, the mean position of the ions also varies when anharmonicity is included. In the frozen phonon approach we are taking, $\langle \Delta x \rangle \neq 0$ implies that the mean position of

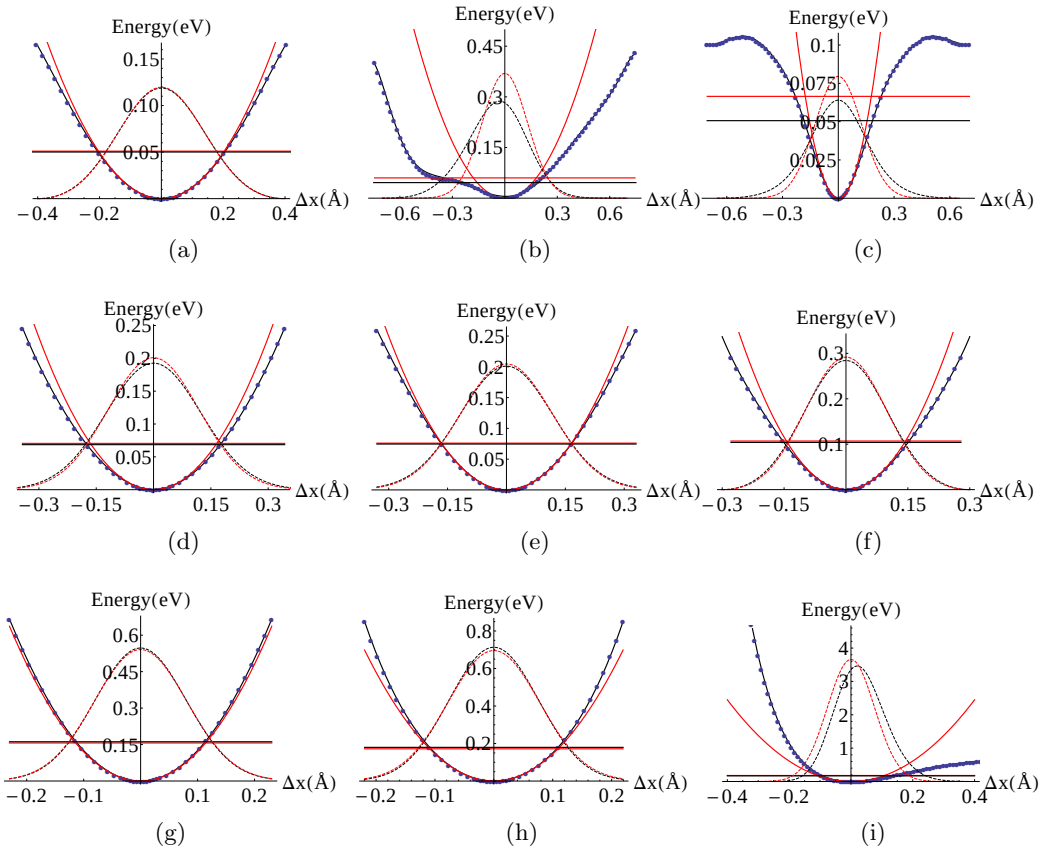

Figure 2.6: Profiles of the potential energy per cell ($U(\Delta x)$) for each of the optical modes, in increasing order of the frequency. The mode displacement Δx, in Å, is the distance that multiplies the corresponding polarization vectors for each mode. Dots represent the computed values, full red lines the quadratic fitting around the minimum and full black lines higher-order polynomial fittings of the computed data. Red (black) horizontal lines represent the ground state energy in the harmonic (anharmonic) case and red (black) dashed lines correspond to the harmonic (anharmonic) ground state wave functions.

the atoms is displaced a distance $\langle \Delta x \rangle$ times the polarization vector of the corresponding mode. Another feature that can be pointed out is the spreading of the wave function compared with the harmonic one when the potential energy curve is wider than the quadratic fitting around the minimum. This is specially evident for the profile (c), and by calculating $\langle (\Delta x)^2 \rangle$ we confirm it (as the potential energy curve is symmetric we have $\langle \Delta x \rangle = 0$).

$$\int \mathrm{d}\,(\Delta x)\,(\Delta x)^2 \left|\varphi_{harm-(c)}\,(\Delta x)\right|^2 = 0.016\ \text{Å}^2 \tag{2.4}$$

$$\int \mathrm{d}\,(\Delta x)\,(\Delta x)^2 \left|\varphi_{anharm-(c)}\,(\Delta x)\right|^2 = 0.027\ \text{Å}^2 \tag{2.5}$$

In the rest of the cases, the wave function obtained by solving the Schrödinger equation

for the fitted potential energy does not differ markedly from the harmonic case.

To finish with this section, let us remark once again that this kind of calculations do not treat the interaction among modes, which is an important part of the anharmonicity. However, we have seen that including the SSCHA treatment of anharmonicity is clearly justified by the characteristics of the obtained potential energy profiles.

2.3.3 Stochastic self-consistent harmonic approximation applied to *Cmca*-4 hydrogen

Now we have seen that anharmonic effects can be important in this system, we are ready to apply the formalism explained in section 1.5.1. The initial guess we have used for the dynamical matrices are the ones calculated by *Quantum Espresso* in a $2 \times 2 \times 2$ mesh of $\mathbf{q}$ points[5]. Thus, the size of the supercell in which forces have to be computed is $2 \times 2 \times 2$ as well. We could have used the dynamical matrices computed in the $6 \times 6 \times 6$ mesh, that have been computed and stored (see Section 2.3.1), but this would considerably increase the computer time because the size of the supercell would be also $6 \times 6 \times 6$, implying calculations on 864 atoms. Nonetheless, one can take advantege of having the $6 \times 6 \times 6$ harmonic dynamical matrices computed. Assuming that

$$\widetilde{\mathbf{D}}^{\,2\times2\times2}(\mathbf{q}) \equiv \mathbf{D}^{\,2\times2\times2}_{SSCHA}(\mathbf{q}) - \mathbf{D}^{\,2\times2\times2}_{harm}(\mathbf{q}) \tag{2.6}$$

is slowly varying in the reciprocal space (which means that the differences between the SSCHA and the harmonic force constant matrices are very localized in the real space) we can interpolate $\widetilde{\mathbf{D}}^{\,2\times2\times2}(\mathbf{q})$ to get $\widetilde{\mathbf{D}}^{\,6\times6\times6}(\mathbf{q})$, and knowing $\mathbf{D}^{\,6\times6\times6}_{harm}(\mathbf{q})$ as we do, we can readily obtain $\mathbf{D}^{\,6\times6\times6}_{SSCHA}(\mathbf{q})$.

We have started the calculation with a first population of $N_c = 50$ configurations. The number of coefficients that have to be minimized is 47: 45 correspond to the force constant matrices, and 2 to the free parameters of the $8f$ Wyckoff position, namely y and z. The first minimization has stopped because $\left|\frac{\rho_{\mathcal{H}_j}}{\rho_{\mathcal{H}_{j_0}}} - 1\right| < \eta \equiv 0.3$, so the initial sampling is not valid anymore. The output of the program gives 6 dynamical matrices and the new equilibrium positions of the ions. New configurations are created using as an starting point the output values of the previous step. This process is continued until we reach a fourth population. Here, the statistical sampling is good and and the minimization is finished because all the coefficients satisfy either condition (a) or (b) from Section 1.5.1 . We increase the number of configurations to reduce the statistical error and get the phonon spectrum converged. The desired convergence is obtained for $N_c = 1500$ configurations. The outputs are the final equilibrium positions of the atoms in the primitive cell and the 6 dynamical matrices in the $2 \times 2 \times 2$ mesh. With (2.6) and

[5]There are 6 independent dynamical matrices on such a mesh, as symmetry operations make some matrices be equivalent.

the exposed interpolation procedure, SSCHA dynamical matrices on a $6 \times 6 \times 6$ mesh are obtained, a total of 52 independent matrices.

Knowing $\mathbf{D}^{6\times6\times6}_{SSCHA}(\mathbf{q})$ the same process to get Fig. 2.4 is followed: we get by interpolation the values of the frequency for **q'** along the symmetry lines. The obtained phonon dispersion is depicted in Fig. 2.7. The most remarkable feature of the phonon spectrum obtained with the SSCHA is the fact that the two branches with highest frequencies, the vibrons, are significantly affected and the frequencies are lowered. Reciprocally, the branch right below the vibrons has higher values for the frequency around the Γ point and near it, vibrons even stand below this branch.

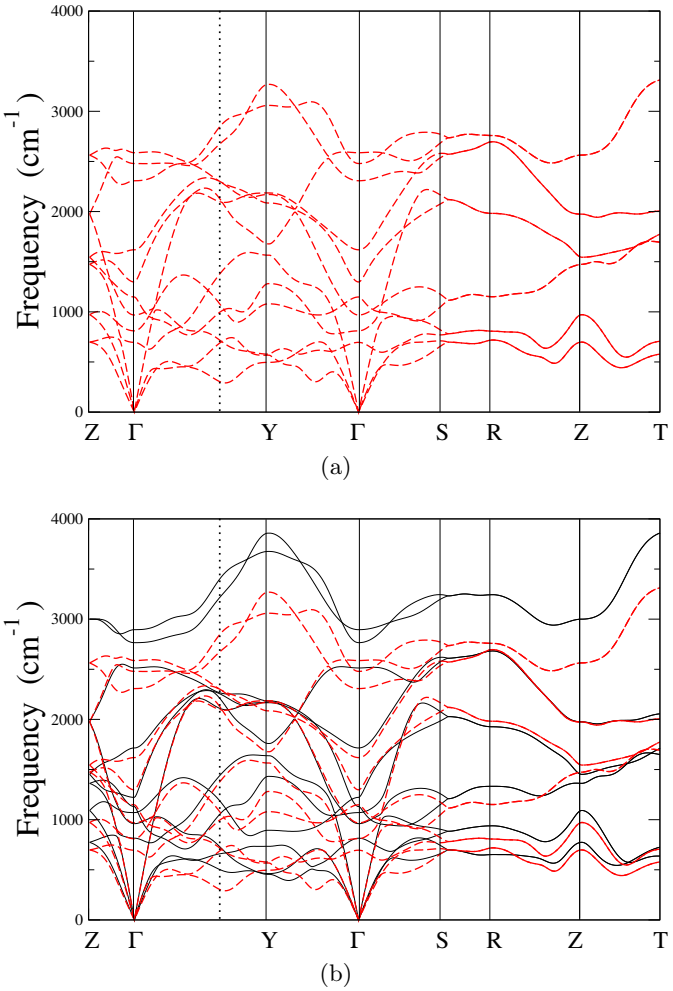

Figure 2.7: (a) Obtained phonon branches with SSCHA method. (b) Comparison of phonon spectrum obtained within the harmonic approximation (black) and the ones obtained with the SSCHA (red).

In Table 2.2 we focus on the changes that have happened at the Γ point, and we compare the values of the frequencies that have been obtained with DFPT in the harmonic

Mode (Fig. 2.3.2)	DFPT	Frozen phonon	SSCHA	Difference (%)
(a)	24.55	30.00	21.01	-14.44
(b)	28.91	29.93	29.14	0.80
(c)	32.23	18.21	24.47	-24.08
(d)	34.04	32.59	38.92	14.34
(e)	36.80	35.07	34.55	-6.11
(f)	51.62	55.30	48.75	-5.56
(g)	75.64	78.11	77.88	2.96
(h)	83.23	89.62	74.61	-10.36
(i)	87.13	73.00	69.62	-20.10

Table 2.2: Obtained frequencies for each of the optical modes at the Γ point, in THz, for the three approximations (DFPT, anharmonic frozen phonon and SSCHA). In the last column, relative difference: $\frac{\text{SSCHA}-\text{DFPT}}{\text{DPFT}}$.

approximation, the values obtained from the anharmonic frozen phonon calculation in Section 2.3.2 and the ones obtained with the SSCHA. We can see that the frozen phonon calculations and the SSCHA do not provide the same values for the frequencies and, what is more, some cases in which the frozen phonon approach foresees an increase of the frequency, the SSCHA does the contrary. This is specially noticeable in the case of (h). SSCHA is, of course, only an approximation, but it takes into account the interaction between modes, whereas the frozen phonon approach does not. We can conclude from Fig. 2.7 and from Table 2.2, where relative differences of the frequencies can be as big as 20% depending on the inclusion or not of anharmonicity, that anharmonic effects are of great importance in this system. Therefore, in an accurate *ab initio* study of this phase of hydrogen anharmonicity should be properly treated.

The effect of anharmonicity that can be observed in Fig. 2.7 is an overall lowering of the frequencies. We try to draw some conclusions about the behavior of T_c by means of a rough estimate based on McMillan's expression [23]:

$$T_c = \frac{\Theta_D}{1.45}\, e^{-\frac{1.04(1+\lambda)}{\lambda-\mu^*(1+0.62\lambda)}} \ . \tag{2.7}$$

In this equation Θ_D is the Debye temperature of the solid, and is related to the typical frequencies of the system. μ^* is an unknown parameter that accounts for the electronic screening, usually of the order of 0.1. Finally, λ is a dimensionless electron-phonon coupling constant defined as

$$\lambda = 2\int_0^\infty \frac{\mathrm{d}\omega}{\omega}\alpha^2(\omega)F(\omega) \ , \tag{2.8}$$

where $\alpha^2(\omega)F(\omega)$ is the Eliashberg function. From Ref. [10] we see that the value for λ, computed within the harmonic approximation for phonons, is around unity, and can even reach 2 with increasing pressure. In this range of values, an increase in λ produces

an increase in the exponential of equation (2.7). Assuming that T_c is governed by the exponential, we see from (2.8) that, in general, lowering the vibrational frequencies of the solid favors superconductivity. Of course, the effect of $\alpha^2(\omega)F(\omega)$ on λ has to be included, but this is beyond the scope of the work. Our calculations show that anharmonicity lowers the phonon frequencies, so it is feasible that T_c gets even higher than the values got in [10].

The fact that vibron frequencies are lowered is also a signal of the tendency to the disociation of the molecules, which can be related to a phase transition. In this sense, anharmonic effects would lower the value of the pressure that is necessary to achieve a monoatomic phase of hydrogen. Apart from the effect in the frequencies, ions can also change their position due to anharmonicity: remember that in SSCHA the free energy is also minimized with respect to the ionic positions. The symmetry of the crystal is respected, and in the end the atoms are also in $8f$ Wyckoff positions, but now the fractional coordinates are y = 0.365 and z = 0.414. The new positions yield an intramolecular distance for both types of molecules of 0.837 Å, versus the 0.793 Å value previous to the SSCHA treatment. This change in the intermolecular distance is consistent with the above-mentioned disociation effect.

With the hydrogen ions in the new positions, we perform a calculation of the electronic bands (Fig. 2.8) and observe that they cross the Fermi level at more points of the high symmetry lines, giving rise to electron and hole pockets that did not exist before. So, even if the relative change in the ionic positions is only a few percent, the Fermi surface has changed (see Fig. 2.9). Following the identification of bonding and antibonding states of Section 2.2 we now see that the band corresponding to intramolecular antibonding and intermolecular bonding is starting to be occupied.

The fact that varying the ionic positions creates such a significant change in the Fermi surface means that non-adiabatic effects may be important in this system, and that the range of validity of the Born-Oppenheimer approximation (Section 1.1) may be restricted. These non-adiabatic effects are related to the electron-phonon coupling, which is also responsible for the superconductivity. Systems with a high electron-phonon coupling are more prone to exhibit superconductivity but, concomitantly, are worse described by the Born-Oppenheimer approximation that we have assumed correct throughout the work. Escaping this vicious circle would imply the treatment of non-adiabatic effects, a problem that is nowadays very difficult to face. The modification of the Fermi surface will cause a change in the electron-phonon coupling and consequently in T_c, so the way is open to a calculation of the electron-phonon coupling that includes anharmonicity, to estimate a more accurate value of T_c.

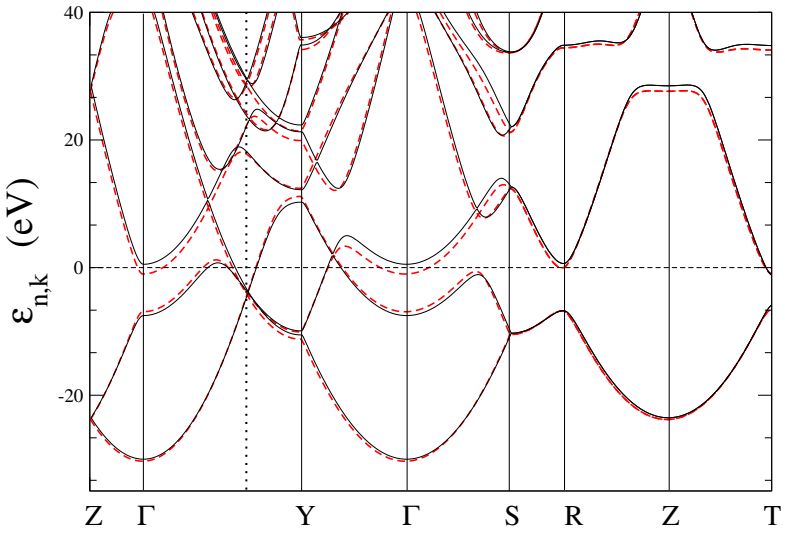

Figure 2.8: Electronic band structure before (after) SSCHA minimization in black (dashed red) lines.

(a) (b)

Figure 2.9: (a) Fermi surface before applying the SSCHA. (b) Fermi surface after applying the SSCHA, with the new ionic positions. The most remarkable feature is that there is an electron pocket around Γ.

Chapter 3

Conclusions

This work has been devoted to the study of the *Cmca*-4 phase of hydrogen at high pressure, which, confirming previous works, has been found to be metallic. In this phase hydrogen still appears in molecules oriented in two directions. The molecular structure can be interpreted in the electronic bands (Section 2.2), and also in the phonon spectrum (Section 2.3.1). The study of the phonons within the harmonic approximation as implemented in *Quantum Espresso* shows two vibron branches that always have higher frequencies than any other branch, and with a significant dispersion, which is an indicator of interaction between molecules of different cells.

We have justified the necessity to treat anharmonicity with a previous analysis of the modes and we have performed anharmonic frozen phonon calculations. In some cases, this kind of calculations predict behaviors that do not coincide with SSCHA calculations, which in principle is more accurate because it also includes the interaction between modes, although it is restricted to harmonic trial Hamiltonians. The inclusion of anharmonicity by means of the stochastic self-sonsistent harmonic approximation modifies the phonon spectrum significantly. The most strongly renormalized branches are found to be the vibrons. A general perspective of the renormalized spectrum shows that the frequencies are overall reduced. Furthermore, the atomic positions vary in a manner that produce new features in the Fermi surface, such as electron pockets around the point Γ. The conclusions that can be drawn from the calculations we have performed can be summarized as follows:

- **Anharmonic effects are important**. The phonon spectrum is significantly modified when anharmonicity is included. Accurate studies of this phase of hydrogen should include anharmonic terms in the treatment of ionic vibrations.
- **Feasibility of an increase in T_c**. Rough arguments following equations (2.7) and (2.8) that do not take into account the effect of the Eliashberg function, lead to the conclusion that lowering phonon frequencies increases T_c.

- **Anharmonic effects tend to lower the pressure necessary to disociate the molecules**. The lowering of the vibron branches and the increased intramolecular distance after the SSCHA treatment point to a structure with less tightly bound molecules. The disociation pressure can be lowered if anharmonicity is included in the calculations.
- **Non-adiabatic and electron-phonon coupling effects may be important**. We have seen that a small variation in the ionic positions causes a considerable change in the Fermi surface, so the ionic movement induces a change in the electronic structure. In such a case, Born-Oppenheimer approximation becomes less valid. On the other hand, the electron-phonon coupling varies when anharmonicity is included, so a new calculation of the Eliashberg function including it is desirable.

A problem that was posed so many decades ago, the metallization and superconductivity in hydrogen, is still nowadays extremely interesting. The increase of computational power and the development in experimental devices bring us closer to the answer, but there is still a lot to do.

Bibliography

[1] J. Dewar, *Sur la solidification de l'hydrogène*, Ann. Chim. Phys. **18**, 145 (1899).

[2] E. Wigner and H. B. Huntington, *On the possibility of metallic modification of hydrogen*, J. Chem. Phys. **3**, 764 (1935).

[3] P. Loubeyre, F. Occelli and R. Letoullec, *Optical studies of solid hydrogen to 320 GPa and evidence for black hydrogen*, Nature (London) **416**, 613 (2002).

[4] N. W. Ashcroft, *Metallic hydrogen: A high-temperature superconductor?*, Phys. Rev. Lett. **21**, 1748 (1968).

[5] P. Pincus, *Superconductivity of Jupiter?*, J. Phys. Colloques **30**, C3-19 (1969).

[6] M. L. Cohen and P. W. Anderson, *Comments on the maximum superconducting transition temperature, in Superconductivity in d- and f-band Metals*, ed. D. H. Douglass (AIP, New York,1972), p.17.

[7] L. Dubrovinsky, N. Dubrovinskaia, V. B. Prakapenka and A. M. Abakumov, *Implementation of micro-ball nanodiamond anvils for high-pressure studies above 6 Mbar*, Nat. Commun. **3**, 1163 (2012).

[8] C. J. Pickard and R. J. Needs, *Structure of phase III of solid hydrogen*, Nature Phys. **3**, 473 (2007).

[9] S. Azadi, B. Monserrat, W. M. C. Foulkes and R. J. Needs, *Dissociation of high-pressure solid molecular hydrogen: a quantum Monte Carlo and anharmonic vibrational study*, Phys. Rev. Lett. **112**, 165501 (2014).

[10] P. Cudazzo, G. Profeta, A. Sanna, A. Floris, A. Continenza, S. Massidda and E. K. U. Gross, *Ab-initio description of high-temperature superconductivity in dense molecular hydrogen*, Phys. Rev. Lett. **100**, 257001 (2008).

[11] I. Errea, M. Calandra and F. Mauri, *Anharmonic free energies and phonon dispersions from the stochastic self-consistent harmonic approximation: Application to platinum and palladium hydrides*, Phys. Rev. B **89**, 064302 (2014).

[12] P. Hohenberg and W. Kohn, *Inhomogeneous electron gas*, Phys. Rev. B **136**, 864 (1964).

[13] W. Kohn and L. Sham, *Self-consistent equations including exchange and correlation effects*, Phys. Rev. A **14**, 1113 (1965).

[14] C. A. Ullrich, *Time-Dependent Density-Functional Theory: Concepts and Applications*, (Oxford University Press, 2012).

[15] N. W. Ashcroft and N. D. Mermin, *Solid State Physics*, (Thomson Learning Inc., 1976).

[16] K. Burke *et al.*, *The ABC of DFT*, http://www.chem.uci.edu/ kieron/dftold2/materials/bookABCDFT/gamma/g1.pdf

[17] J. P. Perdew and Y. Wang, *Accurate and simple analytic representation of the electron-gas correlation energy*, Phys. Rev. B **45**, 13244 (1992).

[18] P. Giannozzi, S. Baroni, N. Bonini, M. Calandra, R. Car, C. Cavazzoni, D. Ceresoli, G. L. Chiarotti, M. Cococcioni, I. Dabo, A. Dal Corso, S. Fabris, G. Fratesi, S. de Gironcoli, R. Gebauer, U. Gerstmann, C. Gougoussis, A. Kokalj, M. Lazzeri, L. Martin-Samos, N. Marzari, F. Mauri, R. Mazzarello, S. Paolini, A. Pasquarello, L. Paulatto, C. Sbraccia, S. Scandolo, G. Sclauzero, A. P. Seitsonen, A. Smogunov, P. Umari, R. M. Wentzcovitch, , *QUANTUM ESPRESSO: a modular and open-source software project for quantum simulations of materials*, J.Phys. Condens. Matter **21**, 395502 (2009).

[19] P. Brüesch, *Phonons: Theory and Experiments I: Lattice Dynamics and Models of Interatomic Forces*, (Springer-Verlag 1982)

[20] S. Baroni , S. de Gironcoli , A. Dal Corso and P. Giannozzi, *Phonons and related properties of extended systems from density-functional perturbation theory*, Rev. Mod. Phys. **73**, 515 (2001).

[21] M. Methfessel and A. T. Paxton, *High-precision sampling for Brillouin-zone integration in metals*, Phys. Rev. B **40**, 3616(1989).

[22] Hooton D. J., *A new treatment of anharmonicity in lattice thermodynamics*, Philosophical Magazine Series **7**, 422 (1955).

[23] W.L. McMillan, *Transition temperature of strong-coupled superconductors*, Phys. Rev. **167**, 331 (1968).